Dynamic Displacement Disorder of Cubic $BaTiO_3$

M. Paściak,[1,*] T. R. Welberry,[2] J. Kulda,[3] S. Leoni,[4] and J. Hlinka[1,†]
[1]*Institute of Physics of the Czech Academy of Sciences, Na Slovance 2, 182 21 Prague 8, Czech Republic*
[2]*Research School of Chemistry, Australian National University, Canberra, ACT 2601, Australia*
[3]*Institut Laue-Langevin, BP 156, 38042 Grenoble Cedex 9, France*
[4]*Cardiff University, School of Chemistry, Park Place CF10 3AT, Cardiff, United Kingdom*

(Received 20 November 2017; published 20 April 2018)

The three-dimensional distribution of the x-ray diffuse scattering intensity of $BaTiO_3$ has been recorded in a synchrotron experiment and simultaneously computed using molecular dynamics simulations of a shell model. Together, these have allowed the details of the disorder in paraelectric $BaTiO_3$ to be clarified. The narrow sheets of diffuse scattering, related to the famous anisotropic longitudinal correlations of Ti ions, are shown to be caused by the overdamped anharmonic soft phonon branch. This finding demonstrates that the occurrence of narrow sheets of diffuse scattering agrees with a displacive picture of the cubic phase of this textbook ferroelectric material. The presented methodology allows one to go beyond the harmonic approximation in the analysis of phonons and phonon-related scattering.

DOI: 10.1103/PhysRevLett.120.167601

The narrow lines of diffuse scattering, discovered half a century ago in x-ray photographs of $BaTiO_3$ crystal, have remained a puzzle for several generations of physicists interested in the nature of ferroelectricity [1–12]. It was soon understood that the observed diffuse scattering reflects a peculiar nanoscale displacement disorder of Ti ions which is intimately related to the ferroelectricity of this classical material [1–3].

An example of such diffuse scattering is the $k = 3$ dark, horizontal straight line in the x-ray diffuse scattering image shown in Fig. 1(a). The analysis of such lines that are evident in experiments with $BaTiO_3$ and related perovskites indicated that Ti ion displacements parallel to a given Ti-O-Ti bond chain are correlated along this chain up to distances of the order of 5–10 nm, while there is little correlation between the displacements perpendicular to the chain [1]. Since then, until the present, these correlated displacements have been considered as the key ingredient in the phase transition of $BaTiO_3$, and they are deemed responsible for a range of nonstandard phenomena occurring even in the paraelectric cubic phase [12–17].

Such correlated displacements, hereafter referred to as chain correlations [1], can be well explained if it is assumed that each Ti cation is at any moment off-centered with respect to the surrounding oxygen octahedral cage, and displaced towards one of its eight facets [1]. The eight-site off-center model gives a tractable framework for many quantitative considerations [1,18–22], and in particular, it allows an explanation to be given as to why these chain correlations eventually vanish in the rhombohedral ground-state phase [1,11,12].

Nevertheless, it has been argued that similar chain correlations might be induced simply by the low-frequency phonon modes [3–6,23–25]. Since the available conventional x-ray scattering data do not provide any direct information about the timescale of the chain correlations, many other techniques have been employed to try to solve this controversy. These efforts yielded conflicting conclusions. On the one hand, many experiments—in particular, the local probe methods—supported the pronounced eight-site off-centering [7,9,18], while the spectroscopic methods designed to probe collective excitations typically indicated that the classical soft-mode picture of the phase transition is more appropriate [25–28].

The most convincing spectroscopic evidence for order-disorder polarization dynamics has been found in the terahertz-range frequency response of the dielectric permittivity of the *tetragonal* ferroelectric phase of $BaTiO_3$ [8]. Its spectrum shows an additional relaxational polar mode, well separated from the three normal IR active phonon modes expected in the cubic perovskite crystal. In addition, theoretical modeling indicated that the characteristic frequency of this extra relaxational polar mode roughly matches the rate of the single-ion hopping between the inequivalent (due to the spontaneous polarization) off-centered Ti positions [8].

In contrast, there is no similarly obvious spectroscopic evidence for the intersite hopping dynamics in the *cubic* phase of $BaTiO_3$. While detailed fitting of the paraelectric soft-mode spectral response with a single damped harmonic oscillator is not fully satisfactory, there is certainly no well-separated central peak in the paraelectric spectra that could be ascribed straightforwardly to the dynamics of the intersite jumps among the eight off-centered Ti positions [28–30]. Moreover, it has not yet been established how the spectroscopic results relate to the diffuse scattering observations: are

 © 2018 American Physical Society

the terahertz-range polar excitations responsible also for the x-ray diffuse scattering planar sheets?

In order to clarify the phase transition mechanism of this textbook ferroelectric substance in a broadly accessible manner, we have collected a comprehensive set of high-resolution x-ray diffuse scattering data covering systematically the whole reciprocal space (up to $Q \approx 6.5$ Å^{-1}). The experiment was carried out at 500 K, i.e., about 100 K above T_C, where most of the recently reported peculiar properties [14,31–34], often forbidden by the cubic symmetry, should be either absent or negligible. A combination of the currently available synchrotron source experimental data with contemporary molecular dynamics modeling yields a very clear-cut picture about the dynamics of the chain correlations in the cubic phase of $BaTiO_3$. In particular, while the planar sheets of x-ray diffuse scattering are shown to be caused by the soft phonon branch scattering, the signatures of a strongly anharmonic local potential with the eight most probable off-centered sites are clearly present in the material as well.

The experimental data were obtained at the Advanced Photon Source 11ID-B beam line using a Perkin-Elmar amorphous silicon detector and an incident x-ray beam with an energy of 58 keV (0.2127 Å). During the measurement, the $BaTiO_3$ single crystal sample, held at the temperature of 500 K, was rotated with $\omega = 0.25°$ steps in a way allowing for systematic coverage of the reciprocal space. The reconstruction of the reciprocal space planes was done with the program XCAVATE [35], after indexing the data within the cubic $Pm\bar{3}m$ spacegroup with the lattice parameter $a = 4.01$ Å and after removal of the known artifacts [36,37]. To the best of our knowledge, such detailed quantitative information about the diffuse scattering in the cubic phase of $BaTiO_3$ has not been reported yet.

Theoretical diffuse scattering intensity maps were derived from computer simulations yielding temporal evolution of atomic positions, contained in a box comprising 50^3 $BaTiO_3$ unit cells. The trajectory was obtained from molecular dynamics simulations conducted with the DLPOLY software [38], using an *ab initio*–based shell-model interatomic potential [39], parameters of which were taken from Sepliarsky *et al.* [40]. The time step was 0.2 fs. After the appropriate equilibration [41], the production trajectory was obtained from about 100 ps of an *NVE* (constant volume–constant energy) ensemble run. The ferroelectric phase-transition temperature in the model occurs at $T_{C,\mathrm{theor}} \sim 300$ K; for a reasonable comparison with the experiment, the calculations were conducted at $T = T_{C,\mathrm{theor}} + 100$ K. Theoretical diffuse scattering intensities were obtained with the DISCUS program [42]. Intensity maps presented in this work were determined as an average of 48 images, each calculated as a cubic average from one snapshot of the structure trajectory. In order to directly identify the dynamics of the scattering processes involved, we have used the information stored in the MD trajectory and numerically evaluated the scattering efficiency at a given momentum transfer $\hbar\mathbf{Q}$ according to the associated energy transfer $\hbar\omega$, in terms of the $S(\mathbf{Q}, \omega)$ scattering function with 0.4 meV energy resolution at several points and paths in the momentum space, using the nMoldyn program [43].

The comparison of the experimental and theoretical results for diffuse scattering intensity distributed within the $hk0$ and $hk1.5$ reciprocal space planes of cubic $BaTiO_3$ is displayed in Fig. 1. The left semicircles of each intensity map in Fig. 1 show experimental results, and the right semicircles show the molecular dynamics prediction.

The integer-coordinate points in the $hk0$ reciprocal space plane correspond to the vertices of the reciprocal lattice of the cubic perovskite structure. The dark diffuse spots located at these reciprocal lattice points are due to the usual thermal diffuse scattering by the thermally activated low-frequency acoustic phonon modes. Each of these spots appears as either an individual elongated ellipsoid or a pair of differently oriented overlying ellipsoids (evoking a butterfly shape). The shape and the orientation of these ellipsoids can be well understood from the anisotropy of the elastic tensor of the cubic $BaTiO_3$ crystal [3,25,45].

There is also a somewhat weaker diffuse scattering intensity emanating from the long axes of the ellipsoidal spots that seems to mutually connect the diffuse spots into continuous diffuse scattering stripes [for example, the $h + k = 4$ intensity stripe in Fig. 1(a)]. More precisely, this weak diffuse scattering intensity is concentrated around all reciprocal space planes coincident with the facets of reciprocal space octahedra, defined by $|h| + |k| + |l| \leq 2n$, where $n = 1, 2, 3$, etc. For example, the diffuse scattering localized near the $h + k + l = 4$ plane appears as the dark

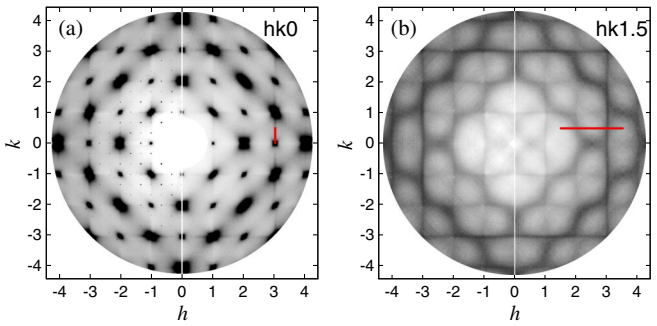

FIG. 1. Diffuse scattering of a cubic $BaTiO_3$ single crystal at $T_C + 100$ K within the (a) $hk0$ and (b) $hk1.5$ planes of the momentum space. The left semicircles show experimental data; the right ones are calculated (see the text). Darker contrast means higher intensity. The vertical and horizontal diffuse lines are caused by the short-range Ti-ion displacement correlations. The two highlighted segments relate to the paths explored in Figs. 3 and 4. The sharp, tiny spots in noninteger positions in the left semicircle of (a) come from $\lambda/3$ contamination of the beam. A larger version of this figure is deposited in the Supplemental Material [44].

streak rippled around the $h + k = 2.5$ reciprocal line in Fig. 1(b), and as the $h + k = 4$ dark streak in Fig. 1(a). It is natural to ascribe these diffuse streaks to the low-frequency phonon modes as well. In fact, the streak intensity roughly scales with the intensity of the adjacent thermal diffuse scattering spots, and the latter follows the known structure factor variation typical for acoustic modes. It has been thus proposed that the streaks and spots are *together* forming an "acoustic component" of the diffuse scattering S_A [3].

In contrast, the scattering related to the Ti chain correlations is restricted to the closest vicinity of the $|h| = n$, $|k| = n$, and $|k| = n$ $(n = 1, 2, 3\ldots)$ reciprocal planes. Consequently, it appears just as a set of extremely narrow intensity lines, parallel to the Cartesian axes in the images of Fig. 1 (the dark horizontal line at $k = 3$, for example). Visibly, the intensity of these lines does not scale with the intensity of the neighboring acoustic diffuse spots. Rather, the observed intensity variations testify that these diffuse lines stem from the disordered opticlike displacements, representing the relative displacement of the Ti ion with respect to the neighboring O and Ba ions [3]. The debated question is whether this optical part of the diffuse scattering, S_O, simply reflects the dispersion of low-frequency soft optic modes, or whether this diffuse scattering arises due to some extra source of Ti chain correlations, which is inherently linked to the eight-site Ti off-centering.

The calculated trajectory allows us to directly inspect the Ti ion displacements with respect to the oxygen octahedral cages. The three-dimensional histogram of the Ti ion's positions with respect to the center of its oxygen octahedron [Fig. 2(e)] shows a very smeared probability distribution, similar to that found in Ref. [46], nevertheless with a shallow local minimum in the center and eight maxima at the anticipated [9,12,18,47] off-center positions. Still, only about 5% of the Ti ions actually fall within these probability peaks; most of the Ti ions are distributed around them.

An example of the instantaneous distribution of the relative Ti-O_6 displacements in real space is shown in Fig. 2(a) (only the y component is displayed). Anisotropic chain correlations between neighboring sites are better revealed in the picture showing displacements averaged over the time of 500 fs [Fig. 2(b)]. For example, the y component of a particular Ti local displacement tends to be parallel to that of its neighbors in the y direction, but there is little correlation in the perpendicular directions [11,48]. Equivalent correlations obviously hold for displacements along the x and z axes. Averaging over a longer period leads to a similar picture, but with a significant reduction of the displacement magnitudes [see the 4 ps averaging in Fig. 2(c)]. This indicates the picosecond lifetime of these correlations.

The dynamical nature of the thermal excitations involved in these Ti correlations can be more quantitatively understood from the frequency dependence of the $S(\mathbf{Q}, \omega)$

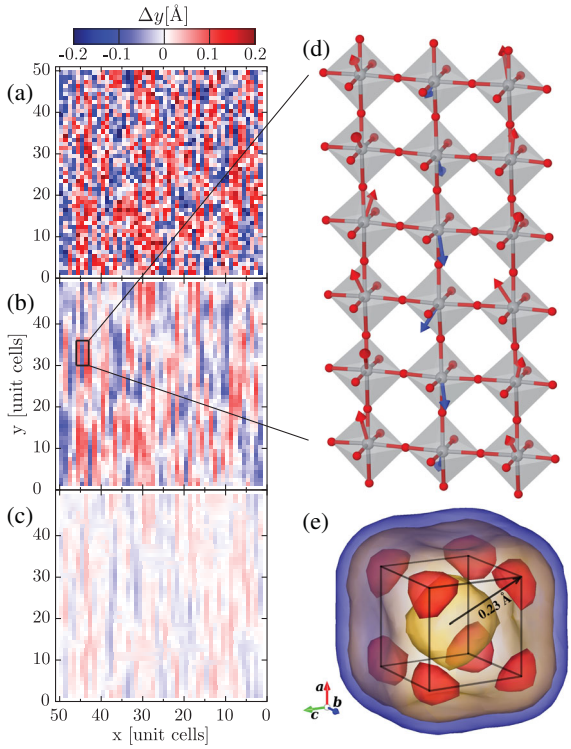

FIG. 2. Distribution of the y components of the relative Ti-O_6 displacement within a selected xy layer of the simulated crystal box: (a) Instantaneous displacements. (b) Displacements averaged over a 500 fs period. (c) Displacements averaged over a 4 ps period. Panel (d) shows a fraction of the simulated atomic structure with arrows showing the magnified vector of the local Ti displacement. (e) Isosurface plot of probability distribution for the Ti atom position with respect to the center of the oxygen octahedron. The average magnitude of the displacement equals 0.147 Å, and the eight most likely positions are marked as corners of the superposed cube with about 0.3-Å-long edges.

scattering function. The profile of $S(\mathbf{Q}, \omega)$ calculated for the [q 0.5 1.5] trajectory in the momentum space is shown in Fig. 3(a). It passes through two S_A stripes located around $q = 2$ and $q = 3$, as well as through the S_O diffuse line at

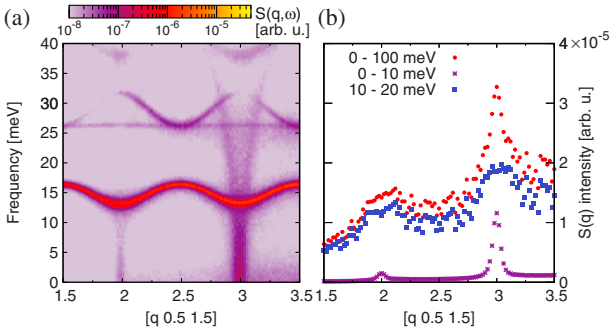

FIG. 3. Dynamical analysis of the diffuse scattering intensity: (a) Map of $S(q, \omega)$ in the [q 0.5 1.5] direction. (b) X-ray scattering intensity determined from integration of $S(q, \omega)$ over the indicated frequency intervals.

$q = 2$ and $q = 3$ [see the segment marked in Fig. 1(b)]. At the simulated temperature, phonons with frequencies above 40 meV are barely populated, so that the overall scattering is given by integration of $S(\mathbf{Q}, \omega)$ over the displayed frequency range. Figure 3(b) shows the full integral as well as the contributions obtained by integration with 0–10 meV and 10–20 meV. Two key conclusions can be drawn here. First, the S_A diffuse scattering stripes are mostly caused by the dispersion of the rather flat phonon branches in the 10–20 meV frequency region [it is barely seen in Fig. 3(a), but the modes with lower frequencies are more populated and thus contribute more to the integral intensity]. Second, the sharp peak at $q = 3$ in Fig. 3(b) arises due to the strongly dispersive phonon branch, apparently dropping from more than 40 meV down to a zero frequency [at $q = 3$; see Fig. 3(a)]. Thus, it is this branch that is behind S_O and the discussed Ti-chain displacement correlations.

Finally, it is interesting to inspect the $S(\mathbf{Q}, \omega)$ scattering function *along* the sheet of diffuse scattering. The $S(\mathbf{Q}, \omega)$ calculated for the [3 q 0] path [Fig. 4(a)] clearly reveals dispersion of both the transverse acoustic branch and an optic branch in the 22–25 meV frequency region. On the top of it, there is a marked scattering component distributed around the zero energy transfer channel ($\omega = 0$), indicating an overdamped or a relaxational mode. The comparison of the S_{BaTi} and S_{TiO} scattering functions, calculated by ignoring O ions and Ba ions, respectively, allows one to conclude that the eigenvector of the excitation involves

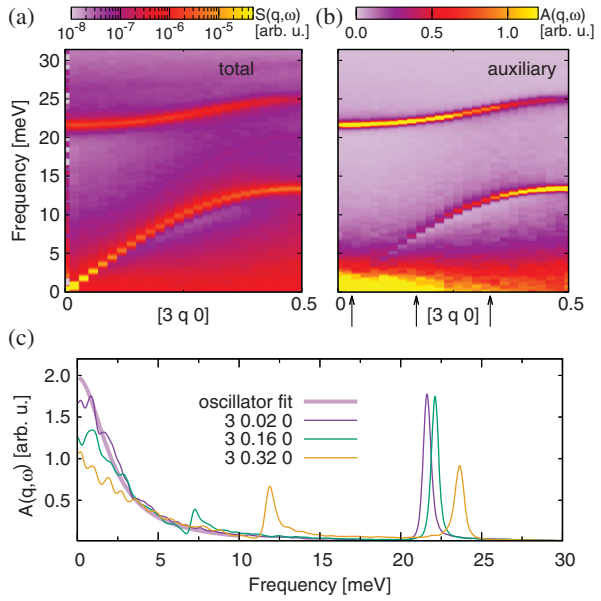

FIG. 4. Dispersion maps in the [3 q 0] direction: (a) Total, displayed using a log scale. (b) Linear combination of partial $S(q, \omega)$: $S_{\mathrm{Ba}} + S_{\mathrm{BaTi}} + S_{\mathrm{Ti}}$, that unveils the optic part of the signal. (c) Optic spectra at different q values indicated by arrows on the map in (b), and a fit to a damped harmonic oscillator described in the text.

mostly out-of-phase motion of Ti and O ions, as expected for the Slater-type order parameter [49,50] of the transition.

In order to eliminate the scattering by low-frequency acoustic mode from the spectra, we have also used partial scattering functions (with contributions only from the indicated ions) to calculate an auxiliary scattering function $A(\mathbf{Q}, \omega) = S(\mathbf{Q}, \omega)_{\mathrm{Ba}} + S(\mathbf{Q}, \omega)_{\mathrm{BaTi}} + S(\mathbf{Q}, \omega)_{\mathrm{Ti}}$. This function suppresses the intensity of the long-wavelength acoustic branch [Fig. 4(b)] so that the spectral shapes of the overdamped opticlike excitation can then be followed even in the closest vicinity of the Brillouin zone center [Fig. 4(c)]. The line shape of the $q = 0.02$ spectrum fits well to that of a harmonic oscillator with a frequency of 7 meV and damping of 25 meV, yielding the 2 meV half width at half maximum (HWHM), implying that the imaginary susceptibility has a maximum around 2 meV [51,52]. This value corresponds to the known position of the soft-mode-related dielectric loss function maximum of $BaTiO_3$ (at $T_C + 100$ K) [27,29,30,52]. In other words, this analysis confirms that the leading contribution to the x-ray diffuse scattering by the Ti-chain correlations coincides with the scattering by the very same terahertz-range soft-phonon branch that determines the high dielectric permittivity of $BaTiO_3$.

The obtained results agree well with a range of previous experiments and calculations—for example, with the inelastic neutron scattering studies [25], EXAFS/XANES spectra [7], and computer simulations [8,29,46,48,53,54]. Some other closely related findings—for example, the detailed line shapes of the terahertz-range dielectric spectra [29,30,55] or NMR spectra (some of which were interpreted using an order-disorder paradigm) [20,22,56] of cubic $BaTiO_3$—were not analyzed here, as it would require still longer simulations times and/or calculations of other quantities. Nevertheless, our results demonstrate that the Ti ion dynamics and diffuse scattering sheets can be well described in terms of anharmonic phonons, and that the intrinsic energy barriers among the off-centered Ti positions are simply too low to stabilize polar clusters at timescales larger then a few picoseconds. We thus hope that this work can be of help in other studies of the polar nanoregions and precursor phenomena in perovskite ferroelectrics.

In summary, this Letter reports synchrotron x-ray measurements of diffuse scattering in the cubic phase of $BaTiO_3$ with extensive momentum space coverage and dynamical contrast. Large-scale molecular dynamics simulations allowed us to calculate maps of diffuse scattering in excellent agreement with those observed experimentally. The calculated high-temperature trajectory provided means for accessing the dynamical profiles of the observed reciprocal space features.

Let us stress that the presented methodology allows one to go beyond the harmonic approximation in the analysis of phonons and phonon-related scattering. This gives us the possibility to clarify several challenging aspects of the

phase transition in $BaTiO_3$. We not only show that the sufficiently soft phonon modes are present there, that their Γ-point spectrum matches the known macroscopic dielectric spectrum, and that the associated dispersion in the momentum space is steep enough to explain the observed sharpness of the diffuse scattering lines, but we also demonstrate that these anharmonic phonons are really the cause of these diffuse scattering lines, in the sense that there is no need for any other comparably intense contribution to be added to make up the observed x-ray diffuse scattering intensity.

This work was supported by the Czech Science Foundation (Project No. 15-04121S). Use of the Advanced Photon Source was supported by the U.S. Department of Energy, Office of Science, Office of Basic Energy Sciences, under Contract No. DE-AC02-06CH11357. The computational part of this research was undertaken at the NCI National Facility in Canberra, Australia, which is supported by the Australian Commonwealth Government. We would like to thank Dr. Aidan Heerdegen for his help during the experiment.

*pasciak@fzu.cz
†hlinka@fzu.cz

[1] R. Comes, M. Lambert, and A. Guinier, Solid State Commun. **6**, 715 (1968).
[2] R. Comès, M. Lambert, and A. Guinier, Acta Crystallogr. Sect. A **26**, 244 (1970).
[3] J. Harada and G. Honjo, J. Phys. Soc. Jpn. **22**, 45 (1967).
[4] A. Hüller, Solid State Commun. **7**, 589 (1969).
[5] J. Harada, M. Watanabe, S. Kodera, and G. Honjo, J. Phys. Soc. Jpn. **20**, 630 (1965).
[6] N. Takesue, M. Maglione, and H. Chen, Phys. Rev. B **51**, 6696 (1995).
[7] B. Ravel, E. A. Stern, R. I. Vedrinskii, and V. Kraizman, Ferroelectrics **206**, 407 (1998).
[8] J. Hlinka, T. Ostapchuk, D. Nuzhnyy, J. Petzelt, P. Kuzel, Ch. Kadlec, P. Vanek, I. Ponomareva, and L. Bellaiche, Phys. Rev. Lett. **101**, 167402 (2008).
[9] S. Ravy, J.-P. Itié, A. Polian, and M. Hanfland, Phys. Rev. Lett. **99**, 117601 (2007).
[10] Y. Liu, R. L. Withers, B. Nguyen, and K. Elliott, Appl. Phys. Lett. **91**, 152907 (2007).
[11] M. Paściak, S. E. Boulfelfel, and S. Leoni, J. Phys. Chem. B **114**, 16465 (2010).
[12] M. S. Senn, D. A. Keen, T. C. A. Lucas, J. A. Hriljac, and A. L. Goodwin, Phys. Rev. Lett. **116**, 207602 (2016).
[13] R. Z. Tai, K. Namikawa, A. Sawada, M. Kishimoto, M. Tanaka, P. Lu, K. Nagashima, H. Maruyama, and M. Ando, Phys. Rev. Lett. **93**, 087601 (2004).
[14] A. M. Pugachev, V. I. Kovalevskii, N. V. Surovtsev, S. Kojima, S. A. Prosandeev, I. P. Raevski, and S. I. Raevskaya, Phys. Rev. Lett. **108**, 247601 (2012).
[15] J.-H. Ko, T. H. Kim, K. Roleder, D. Rytz, and S. Kojima, Phys. Rev. B **84**, 094123 (2011).
[16] V. K. Malinovsky, A. M. Pugachev, V. A. Popova, N. V. Surovtsev, and S. Kojima, Ferroelectrics **443**, 124 (2013).
[17] E. Dul'kin, J. Petzelt, S. Kamba, E. Mojaev, and M. Roth, Appl. Phys. Lett. **97**, 032903 (2010).
[18] R. Pirc and R. Blinc, Phys. Rev. B **70**, 134107 (2004).
[19] M. Kopecký, J. Fábry, and J. Kub, J. Appl. Crystallogr. **45**, 393 (2012).
[20] B. Zalar, V. V. Laguta, and R. Blinc, Phys. Rev. Lett. **90**, 037601 (2003).
[21] H. Takahashi, J. Phys. Soc. Jpn. **16**, 1685 (1961).
[22] B. Zalar, A. Lebar, J. Seliger, R. Blinc, V. V. Laguta, and M. Itoh, Phys. Rev. B **71**, 064107 (2005).
[23] Q. Zhang, T. Cagin, and W. A. Goddard III, Proc. Natl. Acad. Sci. U.S.A. **103**, 14695 (2006).
[24] R. Yu and H. Krakauer, Phys. Rev. Lett. **74**, 4067 (1995).
[25] J. Harada, J. D. Axe, and G. Shirane, Phys. Rev. B **4**, 155 (1971).
[26] H. Presting, J. A. Sanjurjo, and H. Vogt, Phys. Rev. B **28**, 6097 (1983).
[27] H. Vogt, J. A. Sanjurjo, and G. Rossbroich, Phys. Rev. B **26**, 5904 (1982).
[28] K. Inoue and S. Akimoto, Solid State Commun. **46**, 441 (1983).
[29] I. Ponomareva, L. Bellaiche, T. Ostapchuk, J. Hlinka, and J. Petzelt, Phys. Rev. B **77**, 012102 (2008).
[30] J. Weerasinghe, L. Bellaiche, T. Ostapchuk, P. Kuzel, C. Kadlec, S. Lisenkov, I. Ponomareva, and J. Hlinka, MRS Commun. **3**, 41 (2013).
[31] K. Tsuda and M. Tanaka, Appl. Phys. Express **9**, 071501 (2016).
[32] O. Aktas, M. A. Carpenter, and E. K. H. Salje, Appl. Phys. Lett. **103**, 142902 (2013).
[33] M. Roth, J. Tiagunov, E. Dul'kin, and E. Mojaev, J. Cryst. Growth **468**, 753 (2017).
[34] M. Zhang, Z. Guo, R. Tai, H. Luo, K. Namikawa, and J. Cao, Jpn. J. Appl. Phys. **54**, 042401 (2015).
[35] M. A. Estermann and W. Steurer, Phase Transitions **67**, 165 (1998).
[36] T. R. Welberry, *Diffuse X-ray Scattering and Models of Disorder* (Oxford University Press, Oxford, 2004).
[37] T. R. Welberry, D. J. Goossens, A. P. Heerdegen, and P. L. Lee, Z. Kristallogr. **220**, 1052 (2005).
[38] I. T. Todorov, W. Smith, K. Trachenko, and M. T. Dove, J. Mater. Chem. **16**, 1911 (2006).
[39] S. Tinte, M. G. Stachiotti, S. R. Phillpot, M. Sepliarsky, D. Wolf, and R. L. Migoni, J. Phys. Condens. Matter **16**, 3495 (2004).
[40] M. Sepliarsky, A. Asthagiri, S. R. Phillpot, M. G. Stachiotti, and R. L. Migoni, Curr. Opin. Solid State Mater. Sci. **9**, 107 (2005).
[41] The system was consecutively equilibrated over *NST* (constant stress–constant temperature) and *NVT* (constant volume–constant temperature) ensembles for stabilization of volume and temperature, respectively. As a slow drift of shell temperature has been observed, the shells have been allowed to reach the equilibration temperature.
[42] T. Proffen and R. B. Neder, J. Appl. Crystallogr. **30**, 171 (1997).
[43] K. Hinsen, E. Pellegrini, S. Stachura, and G. R. Kneller, J. Comput. Chem. **33**, 2043 (2012).

[44] See Supplemental Material at http://link.aps.org/supplemental/10.1103/PhysRevLett.120.167601 for a larger version of the Fig. 1.
[45] B. Wehinger, A. Mirone, M. Krisch, and A. Bosak, Phys. Rev. Lett. **118**, 035502 (2017).
[46] Y. Qi, S. Liu, I. Grinberg, and A. M. Rappe, Phys. Rev. B **94**, 134308 (2016).
[47] V. Polinger, J. Phys. Conf. Ser. **428**, 012026 (2013).
[48] G. Geneste, J. Phys. Condens. Matter **23**, 125901 (2011).
[49] J. C. Slater, Phys. Rev. **78**, 748 (1950).
[50] J. Hlinka, J. Petzelt, S. Kamba, D. Noujni, and T. Ostapchuk, Phase Transitions **79**, 41 (2006).
[51] A. Al-Zein, J. Hlinka, J. Rouquette, and B. Hehlen, Phys. Rev. Lett. **105**, 017601 (2010).
[52] Additional simulations at 50 K and 200 K above T_C confirmed that this HWHM is roughly proportional to $T - T_C$, as in the experiments.
[53] S. Tinte, M. G. Stachiotti, M. Sepliarsky, R. L. Migoni, and C. O. Rodriguez, Ferroelectrics **237**, 41 (2000).
[54] M. J. Noordhoek, V. Krayzman, A. Chernatynskiy, S. R. Phillpot, and I. Levin, Appl. Phys. Lett. **103**, 022909 (2013).
[55] L. Xie, Y. L. Li, R. Yu, and J. Zhu, J. Appl. Phys. **109**, 054101 (2011).
[56] E. A. Stern, Phys. Rev. Lett. **93**, 037601 (2004).